Topics in Catalysis

The Effect of Potassium on TiO2 Supported Bimetallic Cobalt-Iron Catalysts

--Manuscript Draft--

Manuscript Number:	TOCA-D-20-00147R1
Full Title:	The Effect of Potassium on TiO2 Supported Bimetallic Cobalt-Iron Catalysts
Article Type:	S.I. : Norbert Kruse at 70
Funding Information:	MATTM (MAE01054762018) — Dr. Anna Maria Venezia
Abstract:	The effect of potassium addition on Fischer-Tropsch catalysts containing 10 wt% cobalt and 2 wt% iron supported on pure TiO 2 was studied using a continuous flow reactor at atmospheric pressure, a syngas feed with H 2/ CO =1.7 and GHSV syngas = 1944 mL syngas g cat -1 h -1 . The FTS reaction was performed in a range of temperature 275 - 350°C. Differences in textural, structural, chemical and redox properties of the materials were evaluated by N 2 adsorption/desorption isotherms, XRD, XPS, and TPR. As compared to the catalyst without potassium, forming large quantity of methane at each of the three temperatures, the potassium promoted catalysts formed less methane and consistent amount of alcohol especially at 275 °C. Moreover, the potassium containing samples produced more of the heavier hydrocarbons and more CO 2 at the higher temperatures as compared to the potassium free sample. According to the structural- activity relationship potassium acted as both, structural and electronic modifier.
Corresponding Author:	Anna Maria Venezia, PhD Istituto per lo studio dei materiali nanostrutturati Consiglio Nazionale delle Ricerche ITALY
Corresponding Author Secondary Information:	
Corresponding Author's Institution:	Istituto per lo studio dei materiali nanostrutturati Consiglio Nazionale delle Ricerche
Corresponding Author's Secondary Institution:	
First Author:	Marco Russo, PhD
First Author Secondary Information:	
Order of Authors:	Marco Russo, PhD Valeria La Parola, PhD Giuseppe Pantaleo, Chem.Eng Maria Luisa Testa, PhD Ankur Bordoloi, PhD Rishi Kumar Gupta, Dr Rajaram Bal, PhD Anna Maria Venezia, PhD
Order of Authors Secondary Information:	
Author Comments:	This submission follow a personal invitation for contribution to the special issue in honor of Prof. Norbert Kruse's 70 birthday
Response to Reviewers:	Dear Editor Thank you for the reviewing process of the manuscript" The Effect of Potassium on TiO2 Supported Bimetallic Cobalt-Iron Catalysts. We are grateful to all the referees for the stimulating comments and for the suggestions. As required, we attach a list with the original referee's questions in normal character

	and our answers in italic character. Moreover, in the same list we have included all the changes highlighted with bold characters. All the modified and newly added sentences in the revised manuscript are also highlighted in bold characters. Thank you again for your consideration. Best regards Anna Maria Venezia

The Effect of Potassium on TiO_2 Supported Bimetallic Cobalt-Iron Catalysts

Marco Russo[1], Valeria La Parola[1*], Giuseppe Pantaleo[1], Maria Luisa Testa[1], Ankur Bordoloi[2], Rishi Kumar Gupta[2], Rajaram Bal[2], Anna Maria Venezia[1•]

[1] *ISMN-CNR, Via Ugo La Malfa 153, 90146 Palermo, Italy*

[2] *Indian Institute of Petroleum, Dehradun, Uttaranchal, India*

The effect of potassium addition on Fischer-Tropsch catalysts containing 10 wt% cobalt and 2 wt% iron supported on pure TiO_2 was studied using a continuous flow reactor at atmospheric pressure, a syngas feed with H_2/CO =1.7 and $GHSV_{syngas}$ = 1944 $mL_{syngas}\ g_{cat}^{-1}\ h^{-1}$. The FTS reaction was performed in a range of temperature 275 °C- 350°C. Differences in textural, structural, chemical and redox properties of the materials were evaluated by N_2 adsorption/desorption isotherms, XRD, XPS, and TPR. As compared to the catalyst without potassium, forming large quantity of methane at each of the three temperatures, the potassium promoted catalysts formed less methane and consistent amount of alcohols. Moreover, the potassium containing samples produced more of the heavier hydrocarbons and more CO_2 at the higher temperature as compared to the potassium free sample. According to the structural- activity relationship potassium acted as both, structural and electronic modifier.

Keywords: Fischer-Tropsch; TiO_2 supported CoFe catalysts; K effect, atmospheric pressure

• Corresponding author: E-mail address: annamaria.venezia@cnr.it
*Corresponding author: E-mail address: valeria.laparola@cnr.it

Introduction

The industrial interest in Fischer- Tropsch synthesis (FTS) for the production of transport fuels is nowadays increasing due the stringent need for more sustainable fuels derived from recyclable biomass and also due to the depletion of conventional fossil fuels reserves [1]. The FTS process consists of a catalyzed polymerization reaction, starting from synthesis gas, i.e. a mixture of H_2 and CO, leading to the formation of hydrocarbons of different chain length and water [2]. Ultra-clean fuel, high cetane number of the final liquid products, virtually zero emissions of sulphur compounds and aromatic hydrocarbons are some of the significant advantages of fuels derived from F-T clean technology. Moreover, the emission of particulate matter from an engine fueled with FT derived fuels is lower than from an engine fueled with conventional diesel [3,4]. The catalysts used for FTS reaction are mainly based on cobalt and iron because of the good compromise between conversion efficiency and cost. Moreover, for BTL (Biomass to Liquid) technology, where the used bio-syngas has a molar ratio < 2, the presence of iron, characterized by a high WGS activity, would enhance the FTS activity and increase the selectivity to the desired C_{5+} products [5, 6]. Sintering of the active species due to a locally increased temperature during the high exothermic FTS process, combined with deposition of carbonaceous compounds at the catalyst surface are the main reasons for the catalytic deactivation. In the case of cobalt, the formation of inert carbides and surface restructuring contribute as well to the catalyst deactivation. In the case of iron, re-oxidation of the metallic iron, of Fe_3O_4 and iron carbide, all of them considered active species, to Fe_2O_3 would lead to catalyst deactivation [6]. In order to improve the catalytic performance of these systems, small amounts of other elements, such as noble metals like gold and silver [7-8] or alkali metals have been added [9-12]. Particularly with the iron catalyst, the product distribution in terms of the chain growth probability α, was found to vary from 0.72 for low potassium content to 0.95 for high potassium [9]. For the cobalt catalysts, the effect of small amount of potassium was more striking. Indeed, at atmospheric pressure, α value increased from 0.75 of the potassium free catalyst to 0.9 for amount of potassium corresponding to an atomic ratio K/Co = 0.04 [9]. At the same time, an increasing K/Co ratio resulted in a decrease of the catalytic activity [9, 11]. Most of the recent investigations on the effect of potassium on FTS catalysts deal with silica or alumina carriers and barely on TiO_2 [11-13]. The authors have recently reported on a proper combination of cobalt and iron, supported on pure TiO_2, as a suitable catalyst formulation for Fischer Tropsch Synthesis reaction performed at atmospheric pressure [14]. The superiority of the bimetallic system as compared to the monometallic iron and cobalt catalysts was attributed to the formation of CoxFey alloy, driven by the microwave assisted preparation procedure, with better active site dispersion and improved sintering tolerance during the FTS reaction. As a

continuation of the previous work, the present study aims to elucidate the effect of potassium as promoter of TiO_2 supported bimetallic CoFe catalysts in FTS conversion and hydrocarbon selectivity. The same successful synthetic procedure and ambient pressure reaction conditions were chosen. The effect of potassium was analysed in terms of structural, morphological and electronic properties changes as detected by the variety of techniques such as XRD, TPR and XPS analyses.

2. Experimental

2.1 Support and catalyst preparation

The TiO_2 support was prepared by a sol-gel procedure in the presence of triblock polymer, Pluronic P123, as reported previously [14]. The supports with 1 wt% and 2 wt% K were prepared by wet impregnation of the home-made TiO_2 with an aqueous solution of KNO_3, followed by drying at 80 °C for 2 h and calcining at 500 °C for 2 h.

The bimetallic catalysts with 10 wt% Co and 2 wt% Fe were prepared by co-precipitation assisted by microwave [14]. Namely, an aqueous solution of iron and cobalt nitrate (20 ml) was added to a suspension of the home made pure TiO_2 or potassium doped TiO_2 in ethanol (40 ml). The metal hydroxides were precipitated by adding dropwise NH_4OH until pH = 9. The obtained slurry was placed inside a conventional household microwave set at a power of 180 Watts and operated in 30 s cycles (on for 10 s and off for 20 s) for a total irradiation time of 10 min. The collected precipitate, washed with distilled water and ethanol, was dried at 100 °C for 1 h and then calcined at 500 °C for 2 h. Catalysts were labeled as 10Co2Fe/TiO_2, 10Co2Fe/1KTiO_2 and 10Co2Fe/2KTiO_2, with the numbers in front of the chemical element representing the element wt%. The given composition in terms of Fe, Co and K content was confirmed by Atomic Emission Spectroscopy (MP-AES 4200 Agilent technologies).

2.2 Catalyst characterization

Specific surface areas and pore volumes were determined from N_2 adsorption –desorption isotherms at -196 °C using a Micromeritics ASAP 2020 equipment, through the Brunauer –Emmett-Teller (BET) method in the standard pressure range 0.05–0.3 P/P^0. Before the measurements, the samples were degassed at 250 °C for 2h. By analysis of the desorption curve, using the BJH calculation method, the pore size distribution was also obtained. The total pore volume (V_p) was evaluated on the basis of the amount of nitrogen adsorbed at a relative pressure of about 0.98.

X-ray diffraction (XRD) analyses were performed with a Bruker goniometer using Ni-filtered Cu Kα radiation. A proportional counter and 0.05° step size in 2θ were used. The assignment of the

crystalline phases was based on the JPDS powder diffraction file cards [15]. Crystallite sizes were estimated from diffraction line widths using the Scherrer equation [16].

The X-ray photoelectron spectroscopy (XPS) analyses were performed with a VG Microtech ESCA 3000 Multilab, using Al Kα radiation (1486.6 eV) from a dual Mg/Al anode. Sample preparation and mounting were as described previously [14]. In selected cases, spectra were recorded also on samples being reduced inside a high pressure chamber directly connected to the analysis chamber, at the same reduction conditions of the catalytic test. All the energies were referred to the Ti $2p_{3/2}$ binding energy taken as internal reference, calibrated for the pure TiO_2 support at 458.8 eV. Qualitative and quantitative analyses of the peaks were performed with the CasaXPS software as before [14]. The binding energy values were quoted with a precision of ± 0.15 eV and the atomic percentage with a precision of ± 10%.

Hydrogen temperature programmed reduction (TPR) measurements were carried out with a Micromeritics AutoChem 2950HP Automated Catalyst Characterization System, equipped with a thermal conductivity detector (TCD). About 0.1 g of sample was used for each measurement. The samples were pre-treated with a mixture of 5 vol % O_2 / He at 50 ml/min, heating up (10 °C/min) to 400 °C and holding at this temperature for 30 min. After lowering the temperature down to room temperature, the gas mixture of 5 vol % H_2 / Ar was introduced at 30 ml/min into the sample tube and was also used as a reference gas. During the analysis, the temperature was increased up to 1000 °C at a rate of 10 °C/min. The effluent gas was analysed with a TCD.

The thermogravimetric analyses (TGA) of the samples after the catalytic reactions were performed in air using the TGA 1 Star System of Mettler Toledo. About 10 mg of sample was heated from room temperature to 100 °C, left at this temperature for 1 h and then heated up to 1100 °C at the rate of 10 °C/min in 30 ml/min of flowing air.

2.3 Catalytic measurements

FTS tests were carried out in a continuous-flow quartz reactor, using the experimental apparatus and operative conditions as described previously [14]. Typically, the tests were performed at atmospheric pressure, using a reaction feed of CO, H_2 and He (CO:H_2:He volume ratio of 1:1.7:2.3) at 30 ml/min, GHSV = 3600 $mL_{feed}\ g_{cat}^{-1}\ h^{-1}$ (corresponding to $GHSV_{syngas}$ =1944 $mL_{syngas}\ g_{cat}^{-1}\ h^{-1}$) in a temperature range 275-350 °C. Prior to reaction, the catalysts were reduced in situ in pure H_2 flow (25 ml/min) at atmospheric pressure for 16 h at 350 °C . The catalytic test for each catalyst was performed at three different temperatures, on a same sample, keeping it at each temperature for 8h, an appropriate time for steady state conditions. The inlet and outlet gas compositions were analysed by a GC previously described in details [14]. The CO conversion was calculated as Xco = 100 x (mol

$_{CO_{in}}$- mol $_{CO_{out}}$) / mol $_{CO_{in}}$. Selectivity to the lower hydrocarbon, S_{Cx}, to CO_2 and to the oxygenates was calculated from the corresponding moles and from the converted CO as S_{Cx} = [xmol $_{Cx}$ /(mol $_{CO_{in}}$ – mol $_{CO_{out}}$)] x 100. Selectivity to hydrocarbons with a number of carbon atoms ≥ 5 was obtained as $S_{C5+} = 100-(S_{C1} + S_{C2-C4} + S_{CO_2})$ [14]. The conversion rates at different temperatures, reported as moles of converted CO per minute and per grams of catalyst were determined after 8 h of time on stream (TOS).

3. Results and Discussions

3.1 Catalytic results

The catalytic performance in terms of CO conversion and product selectivity in FTS reaction at different temperatures and after 8 h of reaction time, are summarized in Table 1. As confirmed from the curves of the CO conversion as function of time, given in Fig. S1 of the supporting information, the results refer to steady state conditions. The CO conversion percentages obtained with the potassium free catalyst ranged from 1.5 to 18 upon increasing temperature. The potassium-doped catalysts, still exhibiting an increase of the CO conversion with temperature, converted less CO as compared to the potassium free catalyst. Such unfavorable effect of the alkali ions on the CO conversion in FTS reaction was also reported with Co/Al_2O_3 catalysts and was attributed to the K poisoning of the cobalt active sites [11, 17]. A bar diagram of the catalyst reaction rates, at three different temperatures, determined as moles of converted CO per gram of catalyst per minute, is given in Fig. 1. The graph showed quite clearly the temperature effect and the potassium effect on the catalytic activity. The selectivity results of Table 1, for clarity sake, were summarized in the bar diagrams given in Fig. 2. As already reported for the $10Co2Fe/TiO_2$ catalyst, although tested for a shorter period of time, CH_4, C_2-C_4 and methanol were the main products at 275 °C [14]. The production of CO_2, already observed with the iron containing catalysts supported on TiO_2, was enhanced in the presence of potassium and was favored by the increasing in temperature. CO_2 formation, in accord with literature, was attributed to the water gas shift (WGS) reaction occurring in parallel with the FTS reaction [18]. Increasing the temperature, longer chain hydrocarbons C_{5+} at the expenses of methane and lighter hydrocarbons formed. The increasing selectivity to the heavier hydrocarbons paralleled the increase of the CO conversion. This outcome was in accord with the polymerization mechanism of the FT synthesis, consisting in the adsorption of CO leading to the formation of C_1 monomers. Indeed, the higher the CO conversion, the larger the C1 monomer concentration and therefore the larger would be the selectivity to longer chain hydrocarbons [13]. Methanol formed, to large extent, with K-containing samples. By increasing the temperature, the

production of methanol decreased. The temperature effect was more severe for the potassium containing catalysts exhibiting a more pronounced drop in methanol selectivity counteracted by the increased CO_2 selectivity. The previous study, conducted also at 1 bar, evidenced the importance of iron for the production of alcohols otherwise not formed with monometallic cobalt catalyst [14]. The 'CO-insertion' mechanism was considered the main reaction pathway leading to the formation of oxygenates with iron catalysts [19]. Proposed as one of the mechanisms for the FTS reaction, it involved a first step of insertion of CO into the metal-H bond, followed by hydrogenations, a subsequent insertion of CO in the metal-carbon bonds and a final step with chain termination. In the presence of alkali ions, a modified "CO insertion "mechanism was proposed in which potassium participated in the catalytic cycle by forming a $Fe\text{-}O^{-}K^{+}$ entity [20]. The increased basicity of the iron complex enhanced the electron donation to the CO antibonding state, then weakening the C=O bond and favoring the subsequent hydrogenation to alcohol [20]. In general terms, these results agreed with a previous study on the effect of potassium over similar catalysts [21]. However, whereas that study attributed the catalytic results exclusively to the K-promoted iron, in the present case the decreased CO conversion and the increased long chain hydrocarbon selectivity was ascribable to the effect of potassium on cobalt, present in large amount at the catalyst surface. Indeed, as reported in literature, potassium might act as a structural or electronic promoter by affecting the particle sizes and, as it will be discussed later, also the crystalline phases of cobalt species [11, 17]. It is worth noting that the addition of potassium, besides causing an increase in CO_2 selectivity, produced also an increase in C_{5+} hydrocarbons and oxygenates [17]. Summarizing the catalytic results, with respect to the unpromoted one, the TiO_2 supported CoFe catalysts promoted with 1 wt% and 2 wt% K, although less active, appeared promising in terms of alcohol and heavier hydrocarbon selectivity, even at the operating low pressure conditions.

In order to check for carbon residue on the catalyst, thermogravimetric analyses (TGA) in air of the samples after completion of the catalytic test, i.e. after the last temperature set of data, were performed. Given the low pressure conditions, the surface of the catalyst was not expected to be extensively covered by carbonaceous products, still as shown in Fig. 3, differences in the TGA curves were observed. The K-free sample, experienced a weight loss of about 20 %. On the contrary, the potassium containing catalysts, regardless the potassium content, underwent a weight loss of about 10 %. The weight loss occurred in a temperature interval of 320 - 450 °C, corresponding to the burning of residual carbonaceous species [22]. The difference in weight loss could be a consequence of the reverse Boudouard reaction. Indeed, the CO_2 produced in large amount with the K-promoted samples, activated by the presence of the alkali ions, might react with the deposited carbon yielding CO and accomplishing a sort of catalyst regeneration [23].

3.2 Characterization results

BET

The list of catalysts and support with the corresponding BET specific surface areas, pore diameters and pore volumes, along with crystallite sizes, is given in Table 2. The N_2 adsorption - desorption isotherms along with the pore sizes distribution are shown in Fig. 4. As already reported for similar catalysts on the same support, the isotherms were of type IV, characteristics of mesoporous materials, with clear hysteresis loops of H1 type [24]. The addition of potassium caused a decrease of the surface area, which increased upon the subsequent precipitation of the metal oxides. Similar effect of potassium on the surface area was reported for silica supported iron catalysts [25].

TPR

TPR analyses were performed in order to investigate the possible effect of potassium on the reducibility of the cobalt iron catalysts. The TPR profiles of the calcined samples are shown in Fig. 5. The profiles of the three catalysts were rather similar with some small differences in the peak positions. The K-free catalyst was characterised by a main peak at 485 °C and a smaller peak at around 294 °C. These peaks, in accord with literature and as recently reported for 10Co2Fe /TiO_2, arose from a reciprocal effect of iron and cobalt interacting together, with the cobalt increasing the reducibility of the iron oxide and the iron playing an opposite effect on the cobalt oxide [14, 26]. Therefore, the low temperature peak included hydrogen uptakes for the reduction of Co_3O_4 to CoO and for the reduction of Fe_2O_3 to Fe_3O_4, whereas the intense peak centred at about 485 °C included the reduction of CoO to Co and also the reduction of Fe_3O_4 to FeO [26]. The profiles of the two potassium - containing samples were very similar to the profile of the pure 10Co2Fe/TiO_2 sample, except for a 50 °C shift of the main peak towards lower temperatures and also a narrowing of the main peak. These features suggested an easier reducibility and a lower spread in the particle size distribution and/or less variation in the degree of interaction between the iron and cobalt species or between metals and support. As previously reported for the K-free catalysts, the hydrogen uptake for all the analysed samples, was lower than what expected from the chemical composition [14]. Such discrepancy was ascribable to the strong metal support interaction effect (SMSI) typical of a support like TiO_2. The strong interaction between metal and support, besides determining metal particle decoration by the support itself, inhibiting the hydrogen adsorption, might cause formation of hardly reducible mixed oxides [27]. In order to check the reduction extent of the isothermal H_2 treatment (16 h at 350°C in flowing H_2) preceding the catalytic test, TPR analyses were repeated on likewise pre-reduced samples. According to the results, only 9% of the 10Co2Fe/2KTiO_2 and 15% of

10Co2Fe/TiO_2 were not completely reduced, suggesting again an enhanced reducibility induced by potassium. However, to this respect, the effect of alkali ion on metal reducibility is rather controversial. In some case it was claimed an increase of the reducibility and in some other case a decrease of the reducibility [10, 28-29]. One of the possible explanation for the slightly increased reducibility observed in the present case for the K-promoted samples could be a weakening of the metal-support interaction induced by potassium.

XRD

The X-ray diffraction patterns of the fresh and spent samples after FTS reaction are shown in Fig. 6. All patterns exhibited reflections due to the anatase and rutile phases of TiO_2. As already reported, the home made TiO_2 support contained a mixture of rutile and anatase phase with about 8% of the rutile fraction which, according to literature had a beneficial effect on the FTS activity of the supported catalysts [30]. The corresponding crystallite sizes of the anatase and rutile, as obtained from Scherrer equation, are also listed in Table 2 for the fresh and for the spent samples. The larger TiO_2 crystallite sizes of the potassium containing supports were likely due to the additional thermal treatment of the potassium loading procedure. A further increase of the TiO_2 sizes was observed in the catalysts. As previously reported, the sizes of both anatase and rutile crystallites diminished in the aged catalysts [14]. Such variation was attributed to a restructuring of the materials occurring during the FTS catalytic test. The diffractograms of the fresh catalysts were quite similar, all contained the characteristic peaks of Co_3O_4 (PDF; 078-1969). Through the Scherrer analysis, sizes of 16 and 11 nm were estimated for the Co_3O_4 crystallites of the K- free and K-doped catalysts respectively. By combining the information from the TPR and XRD, potassium seemed to stabilize smaller Co_3O_4 crystallites while preserving them from strong interaction with the support, therefore favoring their reducibility. With respect to the aged samples, the XRD patterns of 10Co2Fe/TiO_2 after the catalytic reaction, beside the TiO_2 reflections, exhibited peaks at $2\theta = 44.2°$ due to metallic Co (fcc, PDF:015-006) and another peak at $2\theta = 45.1°$ attributed to a cobalt enriched $Co_{0.7}Fe_{0.3}$ alloy (PDF:048-1818). As already reported, the formation of the two metallic species occurred already during the pretreatment reduction giving crystallite of 17 nm size, as obtained from Scherrer analyses[14]. After reaction, sizes to 25 nm and 21 nm for Co and $Co_{0.7}Fe_{0.3}$ respectively were estimated. Quite interestingly, the patterns of the two potassium containing catalysts after the FTS reaction, beside the two peaks belonging to metallic cobalt and iron-cobalt alloy, contained also a peak at $2\theta = 42.7°$. This peak was typical of Co_2C crystallites (PDF: 005- 0704). Therefore, during the FTS at ambient conditions, contrary to the case of the K- free catalyst, part of the metallic cobalt species converted into Co_2C. The formation of cobalt carbide at the operative conditions of 1 atm, was in contrast with

a recent study on Co/TiO_2 FTS catalysts reporting formation of such species only at elevated pressure [31]. According to recent literature, during FTS reaction, Co_2C formed only for H_2/CO ratio of the order of 0.5, being unstable in the presence of excess of H_2 [23]. To evaluate better the structural changes of the selected sample $10Co2Fe/1KTiO_2$ at different stages of its catalytic cycle, the corresponding XRD patterns are compared in Fig. 7. It was evident how, under the isothermal reduction pretreatment, Co_3O_4 converted to metallic cobalt species including the alloyed phase, then after FTS, conversion of the metallic cobalt into Co_2C partially occurred. Such result in a way confirmed what previously reported on the effect of the strong metal – support interaction, suppressing the formation of metal iron carbides [14]. Indeed, the formation of Co_2C under unusual condition of low pressure and high H_2/CO ratio reflected the important role of potassium acting as a structural promoter, reducing the metal-support reaction and favoring the formation of the cobalt carbide. The Co_2C crystallite sizes, as estimated by the Sherrer analysis, were 40 nm and 32 nm in the 1 wt% and 2 wt% K containing samples respectively. The presence of Co_2C, generally acknowledged as active phase in the low temperature water gas shift reaction, could explain the large production of CO_2 with the potassium containing samples [17].

XPS

The surface chemistry of the catalysts was analysed by X-ray photoelectron spectroscopy. The main element binding energies with XPS derived atomic ratios are listed in Table 3. The data refer to the calcined and aged catalysts. As already reported for similar catalysts, the Co $2p_{3/2}$ spin orbit component of the calcined samples contained two contributions attributed to two chemical species, Co^{2+} and Co^{3+} [14]. The Co^{2+} was characterized by the Co $2p_{3/2}$ spin orbit component at a binding energy of 781.2 ± 0.2eV with a related shake up peak about 5 eV towards higher energy. The Co^{3+} species was characterized by Co $2p_{3/2}$ component at 779.8 ± 0.2 eV. The presence of the two chemical components was indicative of Co_3O_4 although the XPS derived Co^{3+}/Co^{2+} atomic ratio was lower than the stoichiometric 2:1 ratio [32]. After catalytic reaction, in spite of the poor quality of the spectra, along with the main Co $2p_{3/2}$ peak of the Co^{2+} species, a Co $2p_{3/2}$ component at lower binding energy of about 778.6 eV, typical of a more reduced cobalt, appeared. The Co 2p spectra of the selected sample $10Co2Fe/2KTiO_2$ referring to the calcined, reduced and spent state, are shown in Fig.8. The spectrum of the reduced sample exhibited the main component at high binding energy, attributed to Co^{2+}, and a component at lower binding energy ascribed to metallic cobalt. After FT reaction, the relative intensity of the spectrum decreased, still exhibiting the oxidized and reduced components. Moving to the Fe 2p XPS results, as seen in Table 3, all the iron containing samples in the calcined state had the Fe $2p_{3/2}$ spin orbit component characterized by two peaks, one at 710. 5 ± 0.3 eV typical of Fe^{2+}, generally accompanied by a small satellite at about 8 eV towards high energy, and another one at 712.2 ± 0.2 eV, due to Fe^{3+} [33]. The spectra were typical of Fe_3O_4 phase. After the catalytic test, the XP signal deteriorated and only the Fe 2p component due

to Fe^{2+} species was barely visible. The larger values of the XPS derived surface atomic ratios, Co/Ti and Fe/Co, as compared to the corresponding bulk ratios, as listed in Table 3, indicated cobalt and iron surface segregation. For further information, the XPS derived atomic concentration and relative atomic ratios, excluding oxygen and carbon, for the fresh catalysts are summarized in Table S1 of the supporting information. Overall, there was no significant difference among the samples. The slightly larger Co/Ti ratio of the K-promoted samples may reflect their smaller Co_3O_4 particle sizes and their slightly larger surface area as compared to the potassium-free sample (see Table 2). Moreover, a layer of surface carbon deposited during the reaction could account for the smaller Co/Ti ratios observed for all the spent samples. After reaction, probably due the predominance of the C 1s peak lying nearby, and also to an inward potassium migration, the K 2p spectra were hardly visible. In accord with a surface buildup of carbon during the reaction, as detected by TGA, the C 1s spectra of the spent catalysts, shown in Fig. S2 of the supported information, along with the spectra of the calcined catalysts, were characterized by a main peak at 284.3 eV, down energy shifted with respect to the adventitious carbon at 285.1 eV detected in the fresh samples. As observed before, such peak was typical of amorphous or graphitic carbon [14, 20]. Other C 1s components at higher binding energy were attributable to species such as C-O and C=O bonds. It was worth noting that the relative amount of deposited carbon (C/Ti atomic ratio) was much lower in K- containing sample as compared to the K- free sample, in accord with the potassium promoted reverse Boudouard reaction as discussed above. Moreover, the absence of a C 1s component at about 283 eV typical of the Co_2C species, detected by the XRD of the K-promoted samples after the catalytic reaction, suggested that the carbide species did not segregate at the sample surface but it was located in the inner part of the sample [34].

Conclusion

The addition of potassium to a bimetallic cobalt iron catalyst supported on TiO_2 had a significant effect on the catalytic activity during FTS tests at atmospheric pressure. Besides the decrease of the CO conversion, an increased selectivity towards the valuable products, i.e. C_{5+} hydrocarbons and oxygenates, at the expenses of methane, was the most important outcome. To this respect, the sample with 1 wt% K was slightly better performing. At the same time, the production of CO_2 increased substantially in the presence of potassium. According to TPR investigation, potassium enhanced the reducibility of the cobalt iron catalyst, restraining the strong metal-support interaction typical of the TiO_2 carrier. Upon reduction, before the catalytic test, the cobalt and the iron oxides of the K-free and K-doped samples transformed into metallic Co and alloyed Co_xFe_y. However, most interestingly, during the FTS reaction only the K- doped samples gave rise to a cobalt carbide species, Co_2C, generally reported to form at high pressure and at a low H_2/CO ratio < 0.5. The presence of this carbide, responsible for the increasing CO_2 production, was the consequence of a weakening of

the strong metal-support interaction mediated by potassium. The increased CO_2 production could have been accountable for an easier removal of carbon through the reverse Boudouard reaction. In conclusion, the potassium added to a cobalt-iron catalyst supported on a reducible oxide as TiO_2 acted as a structural and electronic modifier, allowing a good compromise between activity and selectivity.

Table 1. Catalytic performance in terms of CO conversion and selectivity to different carbon compounds of different catalysts, at three different temperatures, determined after 8 hours of time-on-stream at each temperature.

Catalytic Results	10Co2Fe/TiO_2 (°C)			10Co2Fe/1KTiO_2 (°C)			10Co2Fe/2KTiO_2 (°C)		
	275	*300*	*350*	*275*	*300*	*350*	*275*	*300*	*350*
CO conv (%)	1.5	1.6	18.8	1.0	1.5	11.0	1.1	0.8	9.0
CH_4 (%)	48.6	50.1	22.9	33.0	35.1	20.7	27.9	37.7	26.3
C_2-C_4 (%)	40.6	38.9	12.2	35.5	22.8	8.8	29.9	20.1	9.3
C_{5+} (%)	nd	nd	58.3	nd	21.9	47.6	15.0	23.8	47.2
CH_3OH (%)	8.4	7.1	0.9	15.4	4.6	0.6	12.8	3.4	0.6
CO_2 (%)	2.4	3.9	5.7	16.1	15.6	22.3	14.3	14.9	16.5

Reaction conditions: H_2/CO=1.7, GHSV= 3600 $mL_{feed}\ g_{cat}^{-1}\ h^{-1}$, P =1 atm

Table 2. Surface area (S_{BET}), pore diameter, d_p, and pore volume, V_p, of supports and catalysts as determined from N_2 adsorption-desorption measurements of the calcined samples. The Co_3O_4, the Co_2C, the TiO_2 crystallite sizes, as determined by XRD, are also listed.

Sample	S_{BET} (m^2g^{-1})	d_p (Å)	V_p (cm^3g^{-1})	d_{Co3O4} (d_{Co_2C})[a] (nm)	d_{TiO2}[b] (nm)	
					Anatase	Rutile
TiO_2	27	9	0.08	na	25	55
1K/TiO_2	15	8	0.04	na	45	86
2K/TiO_2	10	13	0.03	na	40	67
10Co2Fe/TiO_2	27	14	0.11	16	38 (37)	67(63)
10Co2Fe/1K-TiO_2	21	16	0.12	11(40)[a]	47 (29)	81(39)
10Co2Fe/2K-TiO_2	24	22	0.18	11(32)[a]	44 (30)	72(49)

[a] Co_2C particle size after reaction

[b] the values in parentheses refer to the samples after FTS reaction.

Table 3. Binding Energies (eV) and Atomic Ratios of the catalysts as calcined and after catalytic test. The values in parentheses refer to the bulk ratios.

Sample	Co $2p_{3/2}$		Fe $2p_{2/3}$		Co/Ti (0.2)		Fe/Co (0.2)		K/Ti	
	calc	*spent*	*calc*	*spent*	*calc*	*spent*	*calc*	*spent*	*calc*	*spent*
10Co2Fe/TiO_2	779.9 781.1	778.4 780.6	710.2 712.4	710.4	1.2	0.4	0.3	0.3		
10Co2Fe/1KTiO_2	779.6 781.4	778.6 780.8	710.7 712.2	710.7	1.6	0.5	0.3	0.3	0.2	nd
12Co2Fe/2KTiO_2	779.9 781.0	778.6 781.0	710.6 712.1	711.4	1.5	0.5	0.3	0.2	0.4	nd

Acknowledgments

The Executive Programme for Cooperation between Italy and India (Prot. No. MAE01054762017) and P.O. FSE 2014/2020 for post graduate scholarship are kindly acknowledged. The authors also acknowledge Dr. F. Giordano and Dr. N.G. Gallì for performing XRD and physisorption measurements.

List of references

1) Shafiee S, Topal E (2009) When will fossil fuel reserves be diminished? Energy Policy 37:181–189.
2) Höök M, Tang X (2013) Depletion of fossil fuels and anthropogenic climate change—A review. Energy Policy 52:797-809.
3) Mahmoudi H, Mahmoudi M, Doustdar O, Jahangiri H, Tsolakis A, Gu S, Wyszynski M L (2017) A review of Fischer Tropsch synthesis process, mechanism, surface chemistry and catalyst formulation. Biofuels Eng 2:11–31.
4) Beyersdorf AJ, Timko MT, Ziemba LD, Bu lzan D, Corporan E, Herndon S C, Howard R, Miake-Lye R L, Thornill K L, Winstead E, Wey C, Yu Z, Anderson B E (2014) Reduction in aircraft particulate emissions due to the use of Fisher-Tropsch fuels. Atmos Chem Phys 14:11-23.
5) Hu J, Yu F, Lu Y (2012) Application of Fisher- Tropsch synthesis in biomass to liquid conversion. Catalysts 2:303-326.
6) Jahangirl H, Bennett J, Mahjoubi P, Wilson K, Gu S (2014) A review of advanced catalyst development for Fisher-Tropsch synthesis of hydrocarbon from biomass derived syn-gas. Catal Sci Technol 4:2210.
7) Chen W, Pestman R, Chiang F-K, Hensen EJM (2018) Silver addition to a cobalt Fisher-Tropsch catalyst, J Catal 366:107-114.
8) Jalama K, Coville N J, Xiong H, Hildebrandt D, Glasser D, Taylor S, Carley A, Anderson J A, Hutchings G J (2011) A comparison of Au/Co/Al2O3 and Au/Co/SiO2 catalysts in the Fisher-Tropsch reaction. Appl Catal A 395:1-9.
9) Davis B H (2007) Fisher-Tropsch Synthesis: Comparison of Performances of iron and Cobalt catalysts. Ind Eng Chem Res 46:8938-8945.
10) Niu L, Liu X, Wen X, Yang Y, Xu J, Li Y (2020) Catalysis Today, Effect of potassium promoter on phase transformation during H_2 pretreatment of a Fe_2O_3 Fischer- Tropsch synthesis catalyst precursor. Catalysis Today 343:101-111.
11) Gavrilovic L, Save J, Blekkan E A (2019) The effect of Potassium on Cobalt-Based Fisher-Tropsch Catalysts with Different Cobalt Particle Sizes. Catalysts 9:351-359.
12) Chernavskii P A, Pankina GV, Kazantsev R V, Eliseev OL (2018) Potassium as aStructural Promoter for an iron/Activated Carbon Catalyst: Unusual effect of Component Deposition Order on Magnetite particle size and catalytic behavior in Fischer-Tropsch Sunthesis. ChemCatChem 10:1313-1320.
13) Barrios AJ, Gu B, Luo Y, Peron DV, Chernavskii PA, Virginie M, Wojcieszak R, Thybaur JW, Ordomsky, VV, Khodakov AY(2020), Identification of efficient promoters and selectivity trends in high temperature Fischer-Tropsch synthesis over supported iron catalysts. Appl Catal B 273:119028.
14) Russo M, La Parola V, Testa M L, Pantaleo G,.Venezia A M, Gupta R K, Bordoloi A, Bal R (2020) Structural insight in TiO_2 supported CoFe catalysts for Fischer–Tropsch synthesis at ambient pressure. Appl Catal A 600 : 117621
15) Inorganic Crystal Structure Database (ICSD) (2014) Karlruhe, Germany.
16) Klug HP, Alexander LE (1974) X-ray Diffraction Procedures for Polycrystalline and Amorphous Materials. 2nd ed. John Wiley and Sons: New York, NY, USA
17) Gnanamani M K, Rao Pendyala V R, Jacobs G, Sparks DE, Shafer WD, Davis BH (2014) Fischer–Tropsch Synthesis: Effect of Halides and Potassium Addition on Activity and Selectivity of Cobalt. Catal Lett 144:1127–1133.
18) Schafer WD, Gnanamani MK, Graham UM, Yang J,. Masuku C M, Jacobs G, Davis BH (2019) Fischer-Tropsch: Product Selectivity- The Fingerprint of Synthetic Fuels.Catalysts 9:259.
19) de Smit E, Weckhuysen B M (2008) The renaissance of iron-based Fischer-Tropsch synthesis: on the multifaceted catalyst deactivation behaviour. Chem Soc Rev 37:2758-

2781.

20) Gaube J, Klein H-F (2008) The promoter effect of alkali ions in Fischer-Tropsch iron and cobalt catalysts. Appl Catal A 350:126-132.

21) Duvenhage DJ, Coville NJ (2005)Effect of K, Mn and Cr on Fischer-Tropsch activity of Fe:Co/TiO_2 catalysts. Catal Lett 104: 129-133.

22) Lin Q, Liu B, Jiang F, Fang X, Xu Y, Liu X (2019) Assessing the formation of cobalt carbide and its catalytic performance under realistic reaction conditions and tuning product selectivity in a cobalt-based FTS reaction. Catal Sci Technol 9:3238–3258.

23) Pereira SC, Ribeiro MF, Bathala N, Pereira M M (2017) Catalys regeneration using CO_2 as reactant through reverse - Boudouard reaction with coke. Greenhouse Gas Sci Technol **7**:843-851.

24) Thommes M, Kaneko K, Neimark AV, Olivier JP, Rodriguez-Reinoso F, Rouqueroi J, Sing KSW (2015) Physisorption of Gases, with Special Reference to the Evaluation of Surface Area and Pore Size Distribution (IUPAC Technical Report), Pure App Chem 87:1051–1069.

25) Farias FEM, Rabelo Neto RC, Baldanza MAS, Schmal M, Fernandez FAN (2011) Effect of K promoter on the structure and catalytic behavior of supported iron-based catalysts in Fischer-Tropsch synthesis. Braz J Chem Eng 28:495-504.

26) Lögdberg S, Tristantini D, Borg Ø, Ilver L, Gevert B, Järas S, Blekkan E A, Holmen A (2009) Hydrocarbon production via Fischer-Tropsch synthesis from H_2-poor syngas over different Fe-Co/γ-Al_2O_3 bimetallic catalysts. Appl Catal B 89:167-182.

27) Tauster S J, Fung S C, Garten RL (1978) Strong Metal-Support Interaction. Group 8 Noble Metal Supported on TiO_2. J Am Chem Soc 100:170−175.

28) Feyzi M, Irandoust M, Mirzael A A, Vahid S (2011) Effects of promoters and calcination conditions on the catalytic performance of iron-manganese catalysts for Fischer-Tropsch synthesis. Fuel Processing Technology 82:1136-1142.

29) Cornaro U, Rossini S, Montanari T, Finocchio E, Busca G (2012) K-doping of Co/Al2O3 low temperature Fischer-Tropsch catalysts. Catal Today, 197:101-108.

30) Shimura K, Miyazawa T, Hanaoka T, Hirata S (2013) Fischer –Tropsch synthesis over TiO_2 supported cobalt catalyst: Effect of TiO_2 crystal phase and metal ion loading. Appl Catal A 460-461:8-14.

31) Cats K H, Weckhuysen B M (2016) Combined Operando X-ray Diffraction/Raman Spectroscopy of Catalytic Solids in the laboratiry: The Co/TiO_2 Fischer-Tropsch Synthesis Catalyst Showcase. ChemCatChem 8:1531-1542.

32) Venezia A M, La Parola V, Liotta L F, Pantaleo G, Lualdi M, Boutonnet M, Jaras S (2012) Co/SiO_2 catalysts for Fischer-Tropsch synthesis; effect of Co loading and support modification by TiO_2. Catal Today 197:18-23.

33) Yamashita T, Hayes P(2008) Analysis of XPS spectra of Fe^{2+} and Fe^{3+} ions in oxide materials. Appl Surf Sci 254:2441-2449.

34) Pei Y, Ding Y, Zhu H, Zang J, Song X, Don W, Wang T, Yan L, Lu Y (2014) Study on the effect of alkali promoters on the formation of cobalt carbide (Co_2C) and on the performance of Co_2C via CO hydrogenation reaction. Reac Kinet Mech Cat 111: 505-520.

Figure captions

Fig. 1. Conversion rate over different catalysts at three different temperatures.

Fig. 2. FTS product selectivity over different catalysts at different temperatures after 8 h of time on stream.

Fig. 3. TGA curves of spent catalysts after the FTS test.

Fig. 4. N_2 adsorption/desorption isotherms and pore size distribution curves (inset) of TiO_2 supported catalysts and corresponding TiO_2 support.

Fig. 5. TPR profiles of the TiO_2 supported catalysts.

Fig. 6. XRD of samples; a) calcined and b) after FTS.

Fig. 7. XRD patterns of the 10Co2Fe/1KTiO_2 as: a) calcined; b) reduced; c) spent.

Fig. 8. Co 2p photoelectron spectra of 10Co2Fe/1KTiO_2 after different stages of its life: a) calcined; b) reduced; c) after catalytic reaction.

Figure 1

Click here to access/download;Figure;Fig. 1.jpg

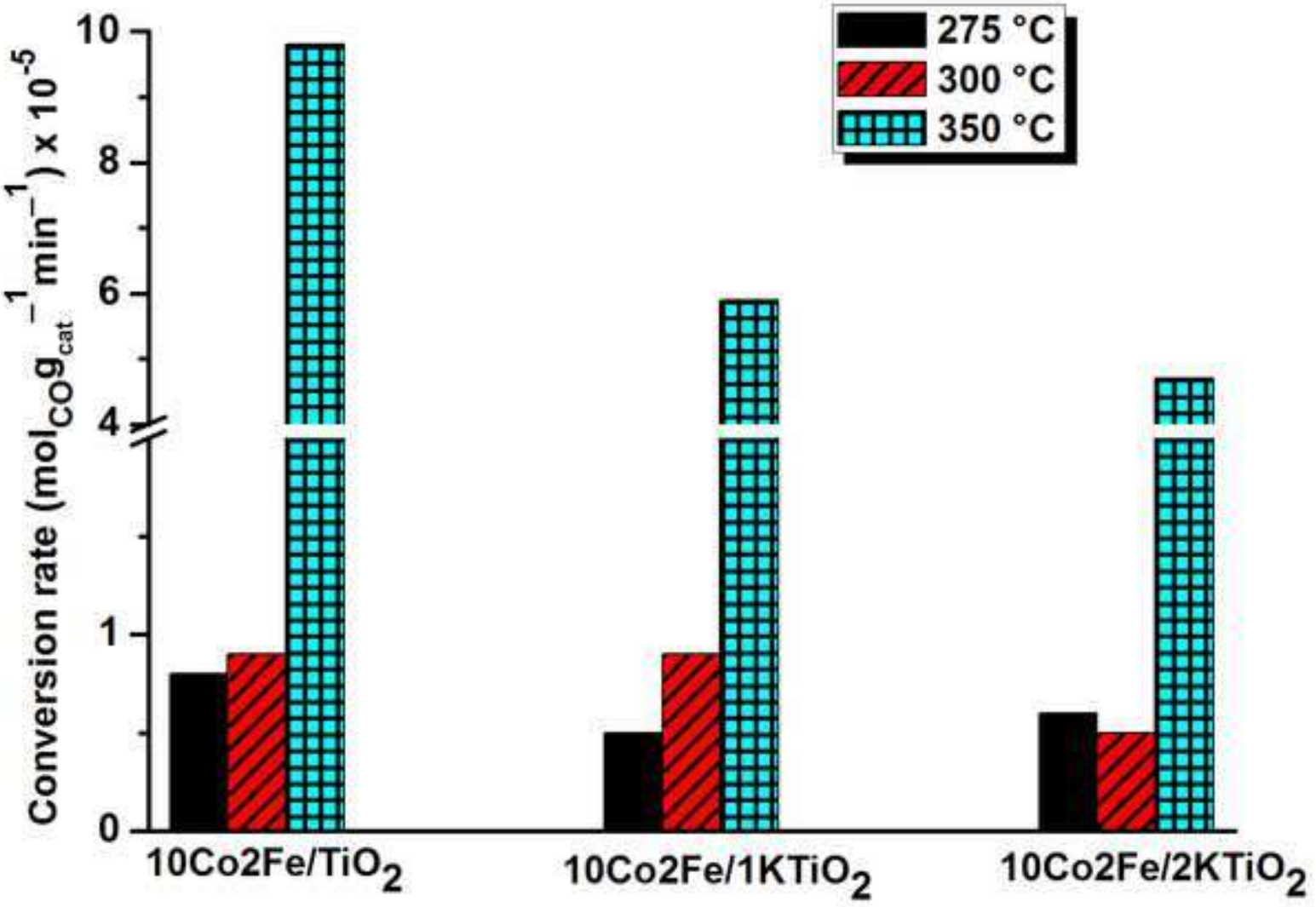

Figure 2 top

Click here to access/download;Figure;Fig. 2 top.jpg

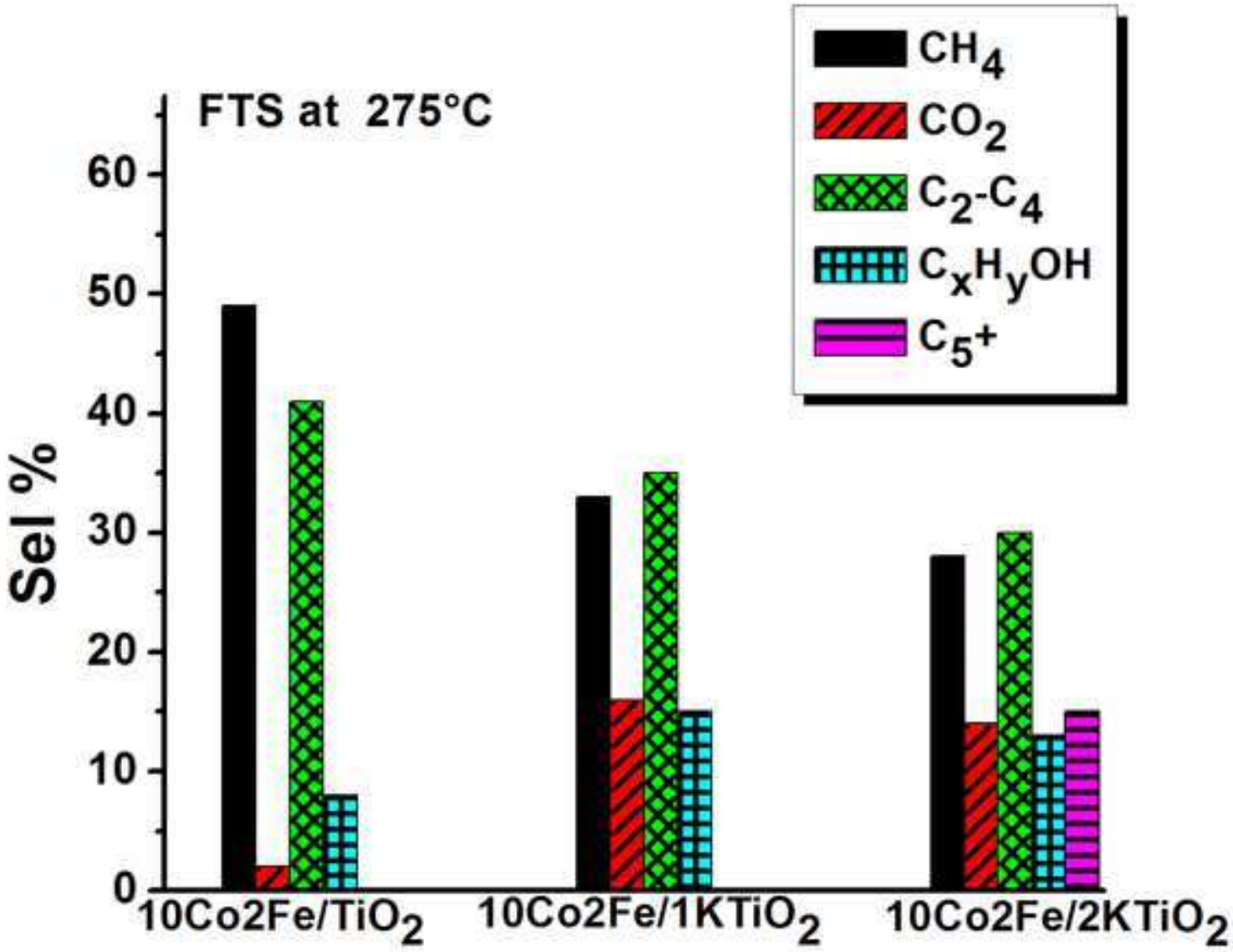

Figure 2 middle

Click here to access/download;Figure;Fig. 2 middle.jpg

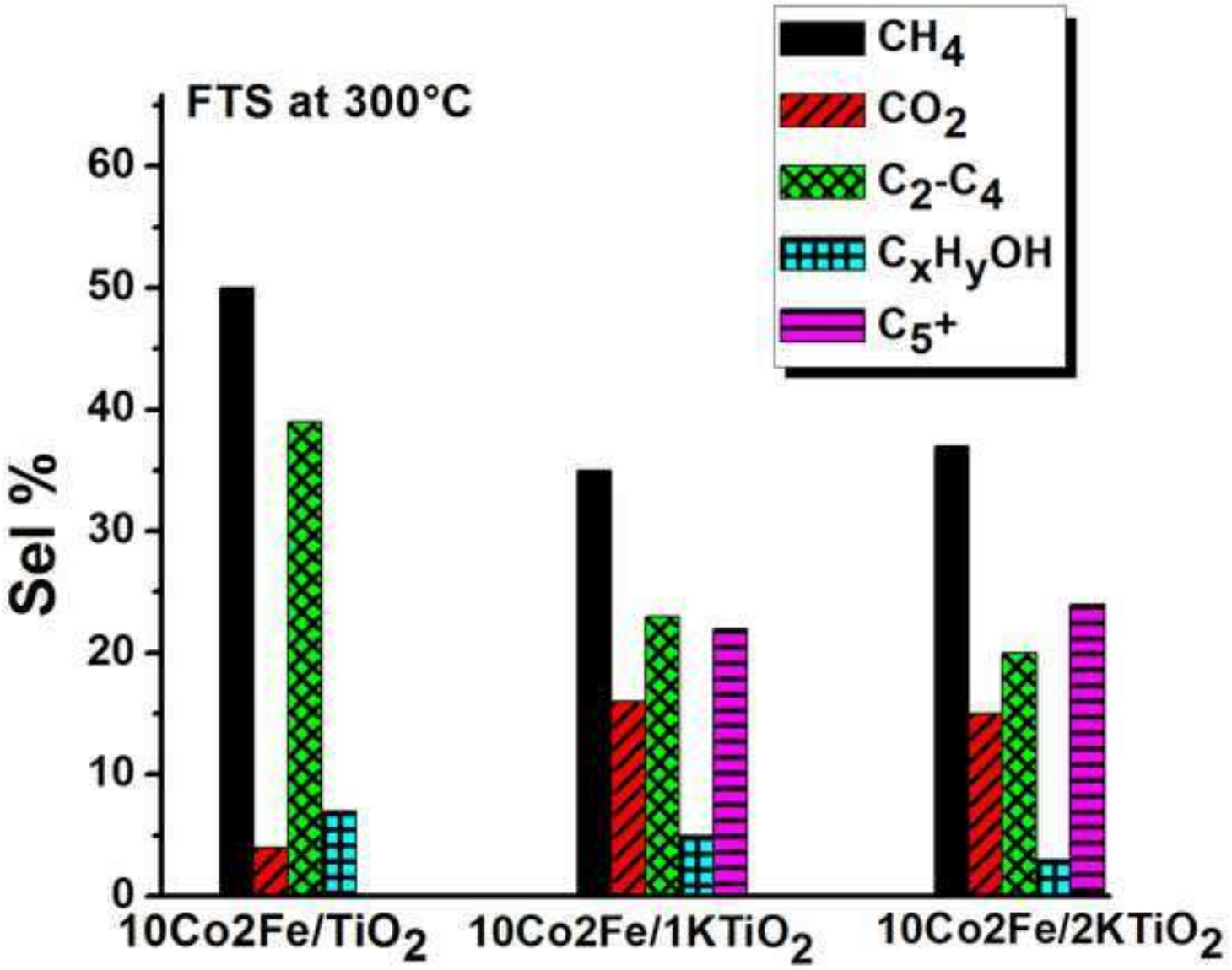

Figure 2 bottom

Click here to access/download;Figure;Fig. 2 bottom.jpg

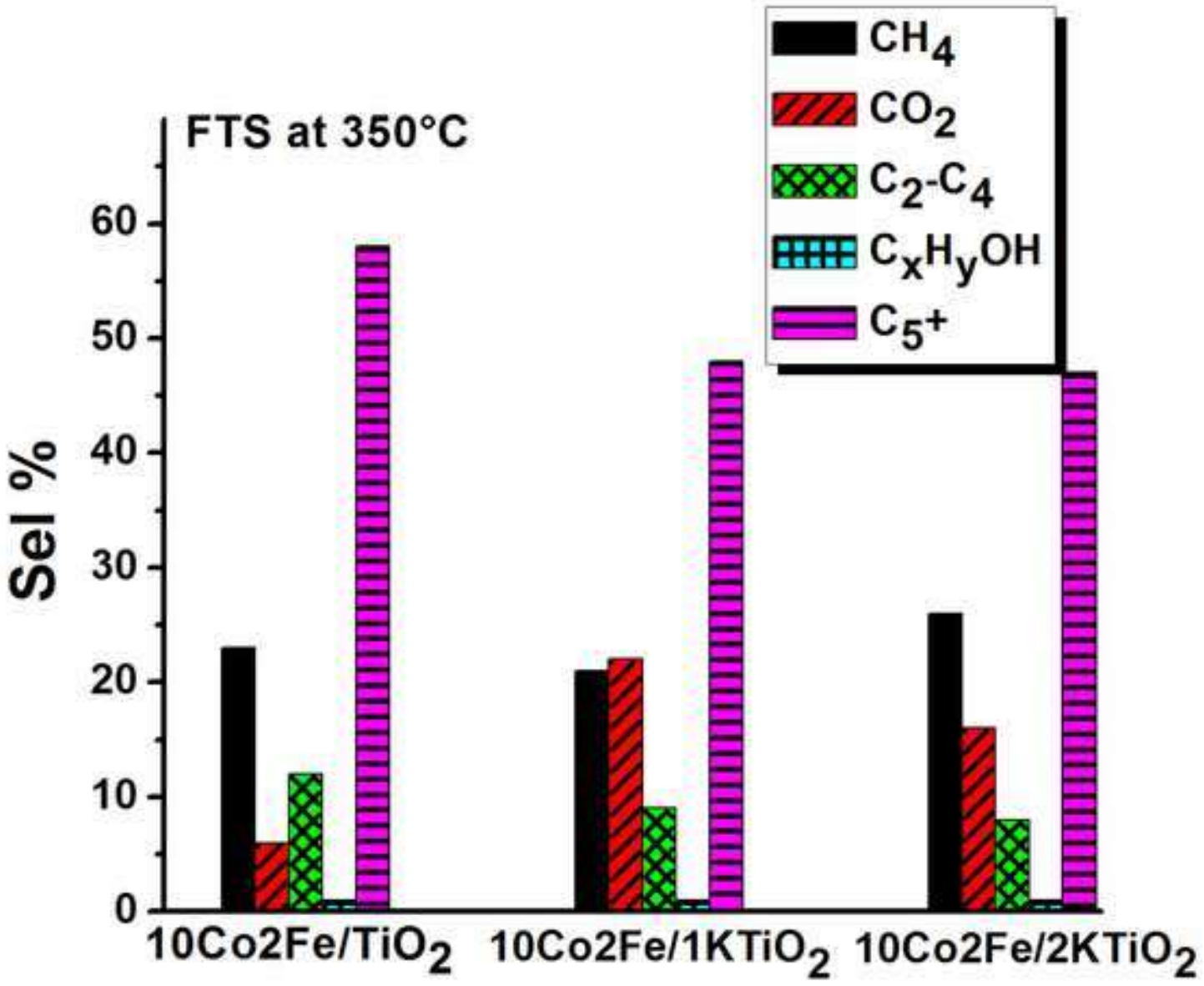

Figure 3

Click here to access/download;Figure;Fig. 3.jpg

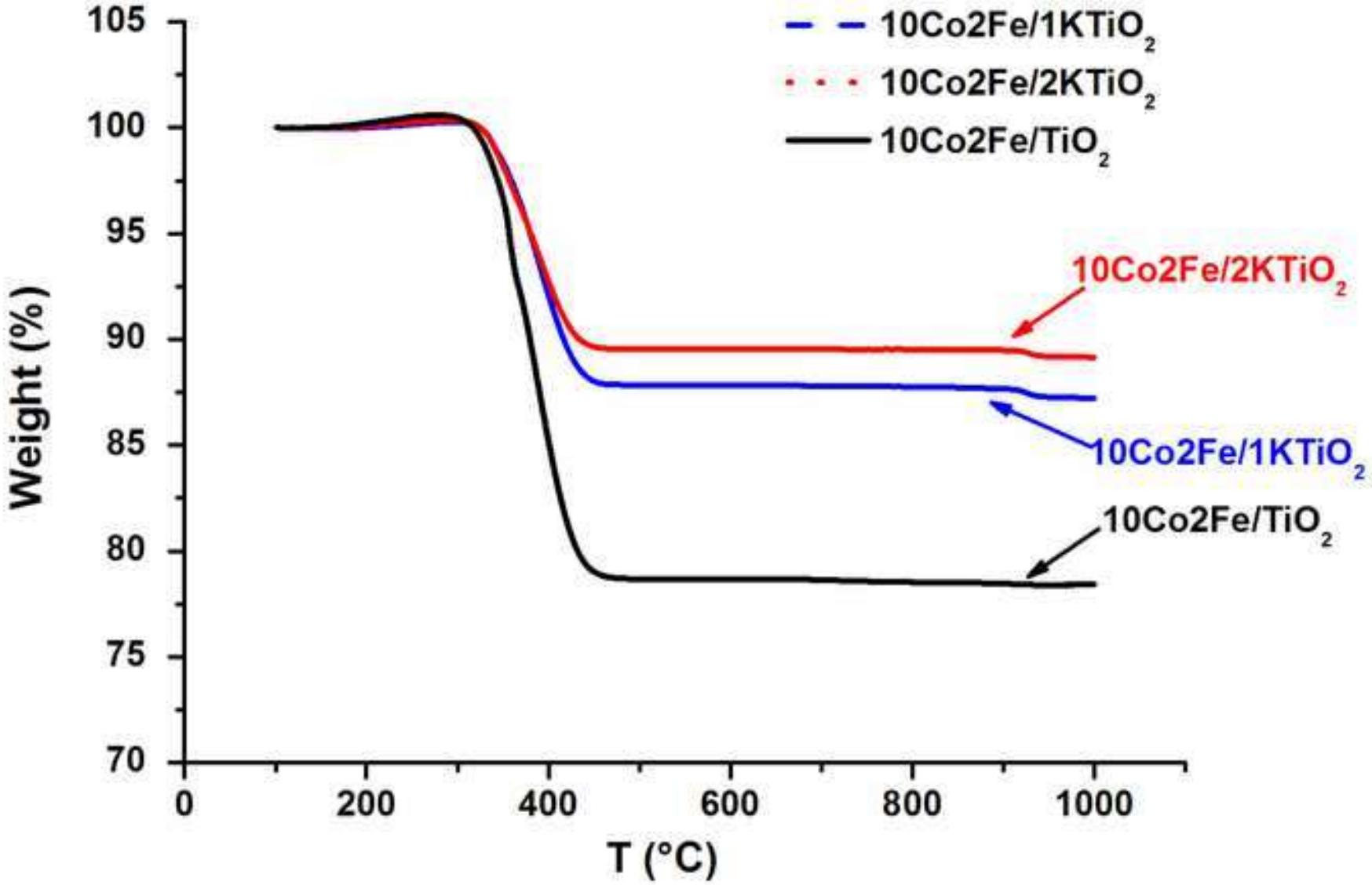

Figure 4

Click here to access/download;Figure;Fig. 4.jpg

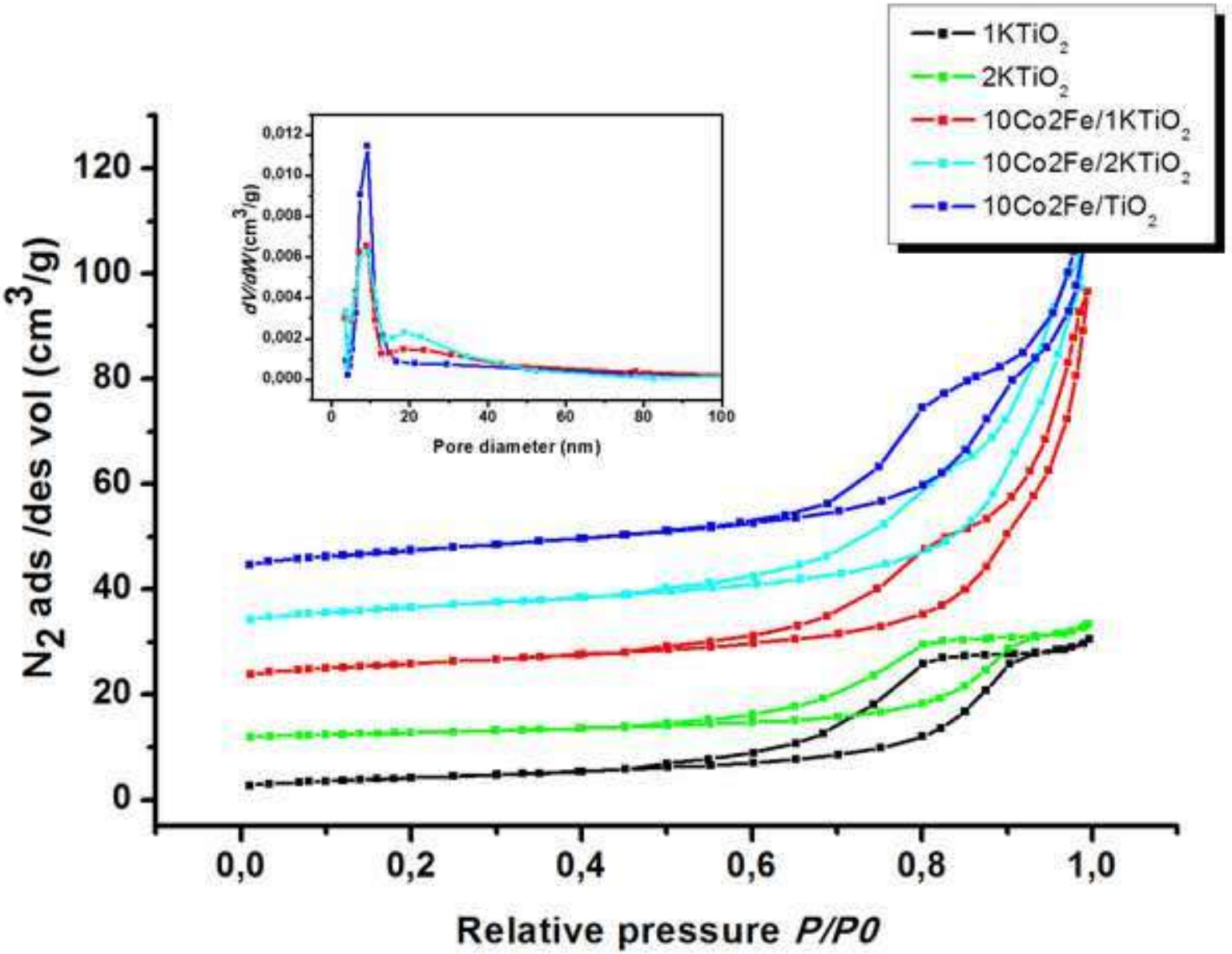

Figure 5

Click here to access/download;Figure;Fig. 5.jpg

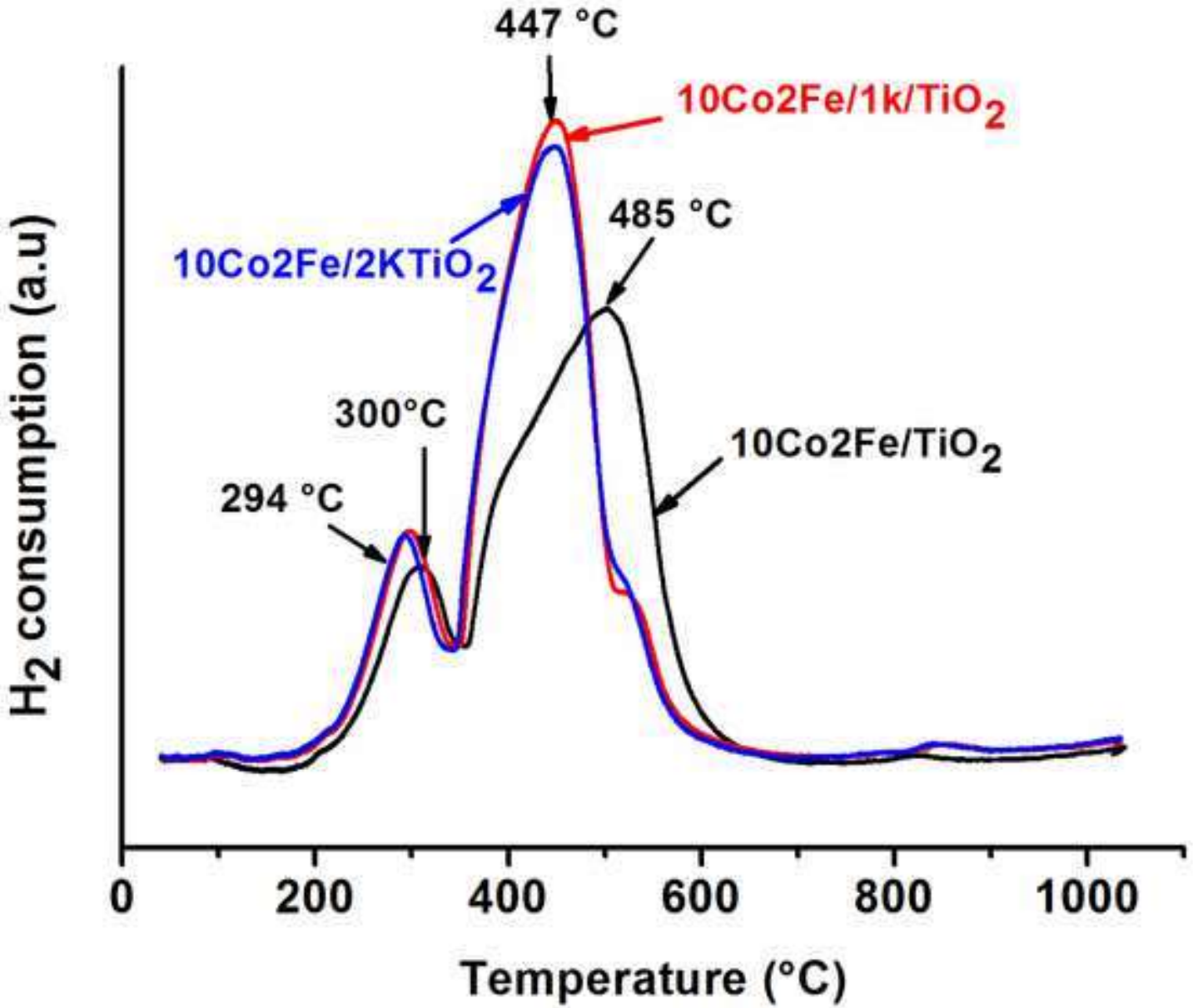

Figure 6

Click here to access/download;Figure;Fig. 6.jpg

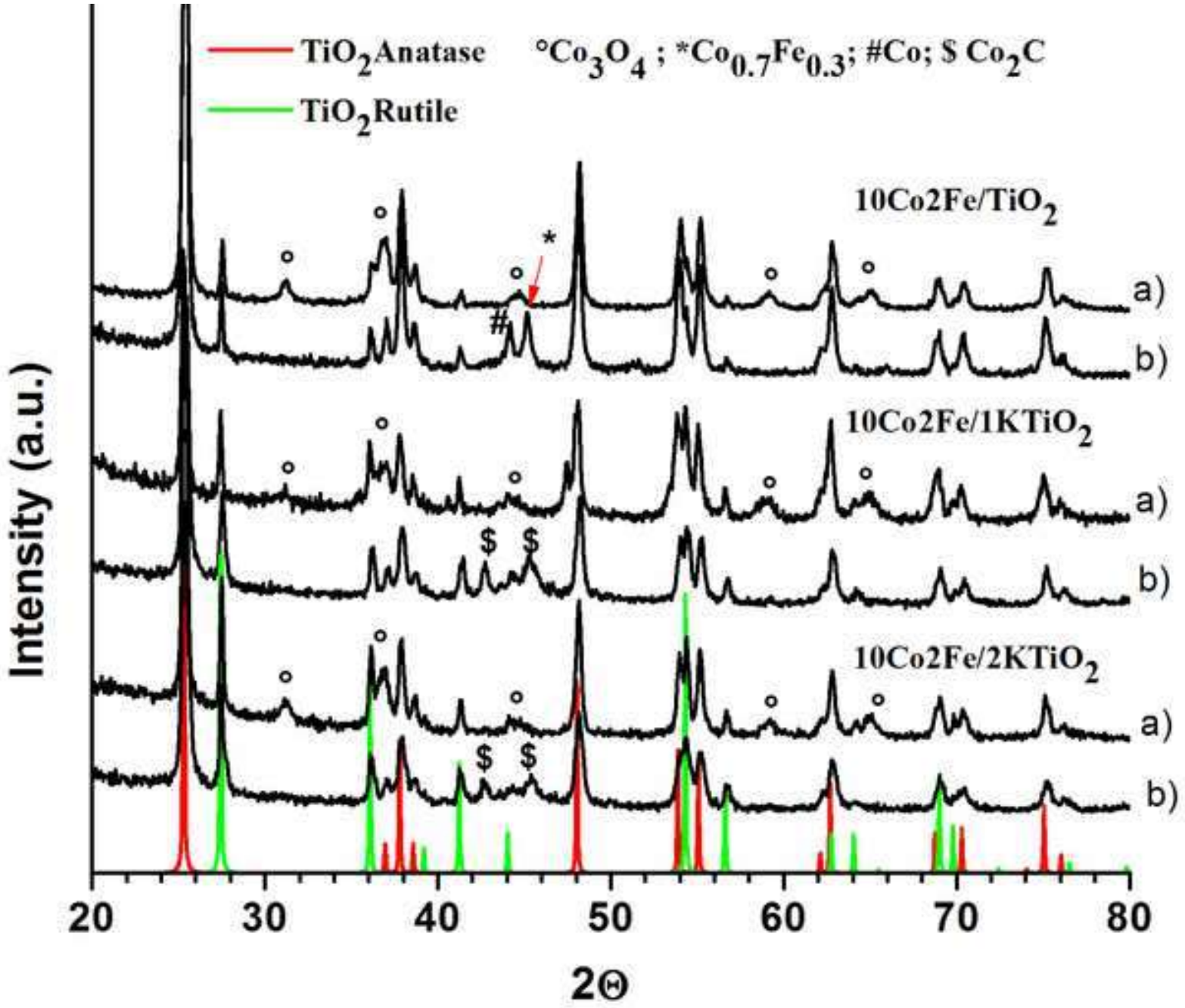

Figure 7

Click here to access/download;Figure;Fig. 7.jpg

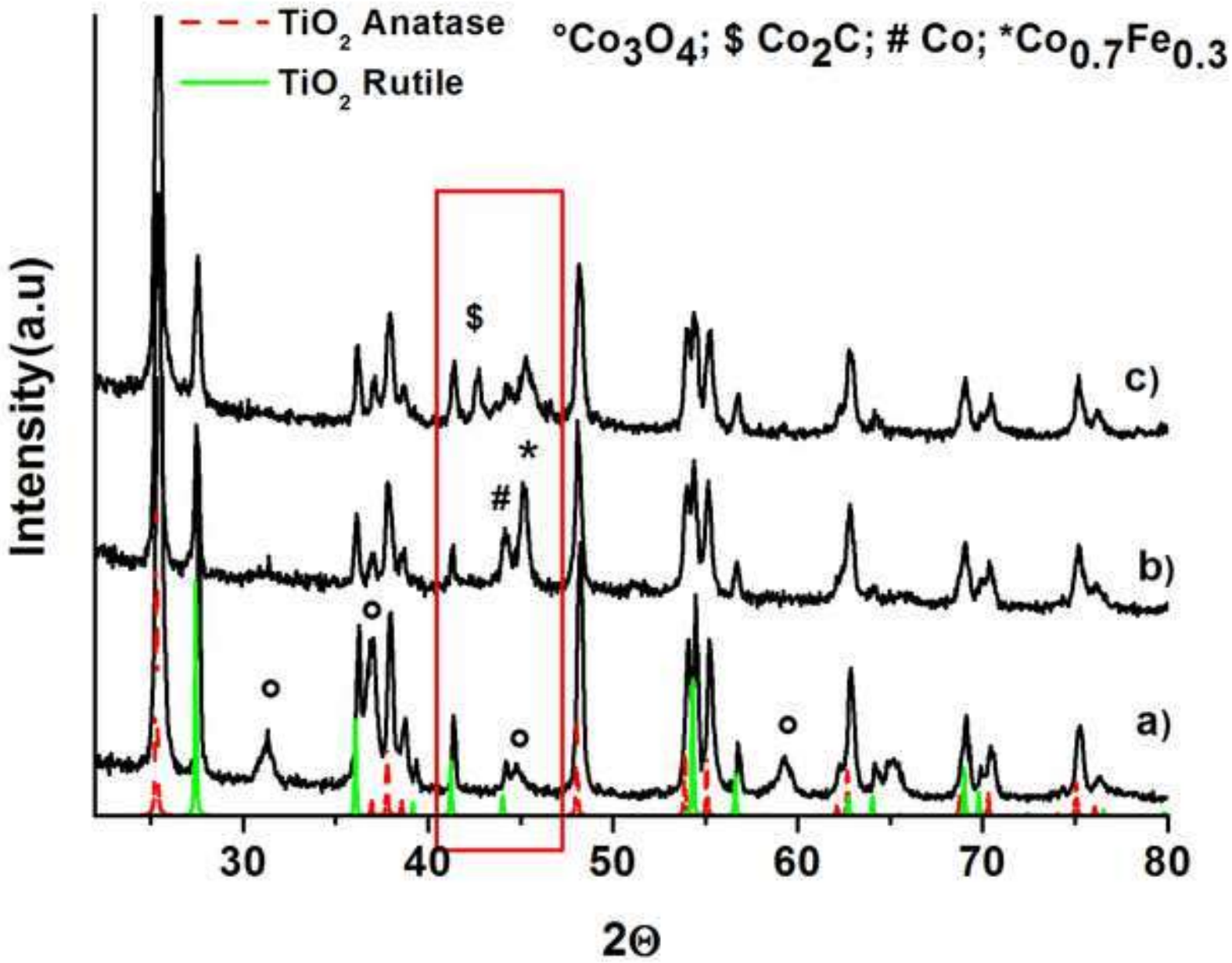

Figure 8

Click here to access/download;Figure;Fig. 8.jpg